Multi-port High Step-up DC/DC Converter for Hybrid Renewable Energy Application

E. Seifi [1], A. Rajaei [2], S. Zare [2], A. Nabinejad [2], S. H. Nobahar[3]

[1] *Department of Electrical and Electronics, Roshdiyeh Higher Education Institute, Tabriz, Iran*
[2] *Electrical and Electronics Department, Shiraz University of Technology, Shiraz, Iran*
[3] *Department of Electrical Engineering, Azarbaijan Shahid Madani University, Tabriz, Iran*

Abstract- *This paper presents a novel multi-port DC/DC converter which is suitable to be used as the interface of hybrid renewable energy systems. The converter contains three unidirectional power flow ports which two of them are input ports and are connected to two independent energy sources while the third one is the output port that feeds a standalone load. Furthermore, the proposed converter contains a bidirectional power flow port to charge/discharge an energy storage system (battery). In addition to multi-port structure, high boost value of voltage gain is the other merit of the converter. Hybrid system is composed of fuel cell (FC), photovoltaic (PV) panels and a battery pack. Different operating states are discussed, and a control system based on decoupling networks is presented. The control system is able to seek and extract maximum power of PV panel, adjust generated power of FC, and handle charging and discharging modes of battery. In order to control operating modes of the proposed converter, a power management method is also presented. By the way, small signal model is presented for the converter. The bode diagram has been plotted from the small signal model. Then the controller it was designed from the bode diagram. The results of simulation by the PI controller are presented. Also, the simulation results by P&O algorithm for the converter has been evaluated. Several Simulation and experimental tests have been carried out to evaluate the analysis and feasibility of the aforementioned system. The results verify well performance of the converter and confirm the simulations and theoretical results.*

KEYWORDS*:* Hybrid renewable energy, Photovoltaic, Fuel cell, DC/DC converter, Multiport converters.

1. INTRODUCTION

Photovoltaic (PV) energy systems is regarded as an important renewable energy resource compared to other types, due to several merits such as availability, noiseless, pollution-free operation, high flexibility and little maintenance [1-4]. However, generated power of PV panels is strongly related to the environmental status such as irradiance, temperature, and unexpected shadows [5], which makes difficulties to supply standalone loads. Therefore, it is inevitable to combine PV panels with other alternative energy sources. Fuel cell (FC) is an outstanding choice because of advantages such as cleanness, reliability and high efficiency. However, the main drawback is slow dynamic response makes

problems particularly at transient conditions [6-8]. A FC stack might not be able to increase its output power and regulate the output voltage fast enough. Therefore, energy storage systems with fast dynamic response (battery) are necessary to be utilized. Hence, in the literature hybrid energy systems using PV/FC/Battery are introduced (Fig. 1) [9-15].

Compared to single-sourced systems, the hybrid power systems provide high quality, more reliable, and efficient power. In these systems storage port should have the bidirectional power flow capability [4], [11-12]. In addition, the power sources should have be able to supply the load individually and simultaneously [13].these multi-port systems are used in electric vehicles or isolated small renewable energy generation based power supplies.

Several converter topologies have been proposed to hybridize energy sources [14-19]. In [20], an intelligent optimal power management with three main benefits including control of temperature fan, fuzzy hydrogen control and adaptive current–voltage

fast-charging control. In [21], a two-layer energy management with minimizing hydrogen consumption is studied.

Traditionally, the different energy sources are coupled in a common DC or AC link. However, such structures suffer from high number of components, control complexity and high cost. Recently, several non-isolated DC/DC converters with multi-input structure have been presented to combine different energy sources [15-16]. These structures are favorable due to their simple structure and control strategy, high reliability and low manufacturing cost.
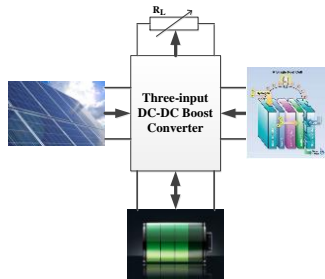
Fig. 1. Hybrid system composed of PV/FC/Battery.

This paper proposes a new boost DC/DC converter with multi-input structure which is suitable for hybridizing PV/FC/ Battery energy sources. As shown in Fig. 1, the presented converter has a bidirectional power flow port and two unidirectional ports. Bidirectional power flow port is used to provide charge/discharge mode for the battery system. There are also several other advantages for the presented converter such as higher output voltage gain, utilizing only one resource in case the other power sources can't provide energy which this capability enhances the safety and reliability of the proposed converter. By proper control of the presented converter, it is aimed to extract power of PV panels as maximum as possible, regulate power generation of the FC and manage the battery charge/discharge modes. Both of power generation sources are able to charge and discharge the battery. Furthermore, to assure efficient performance of the hybrid system, a general power management strategy is given. Finally, in order to evaluate efficiency and practicability of the proposed converter, simulations have been implemented in MATLAB/Simulink software and results are extracted. Bode diagram has been plotted from the small signal model. Then the controller it was designed from the bode diagram. The results of simulation by the PI controller are presented. Also, the simulation results by P&O algorithm for the converter has been evaluated.

2. CONFIGURATIONS, SPECIFICATIONS, AND BASIC OPERATION PRINCIPLES OF THE PROPOSED CONVERTER

The circuit configuration of the proposed multi-port DC/DC boost type converter is shown in Fig. 2 which contains three terminals to connect to two energy sources (PV, and FC) and an energy storage system (battery). The port to which the battery is connected is bidirectional. RL is the resistive load which can also represent an inverter connected to the DC link. The presented structure utilizes three unidirectional power switches (S1, S2, S3) and a bidirectional power switch (S4). There are also three diodes in the structure. The diodes (D1, D2, D3) are in complementary with power switches (S1, S2, S3), respectively. The converter has to work in continuous conduction mode (CCM) as it is connected to PV, and FC, therefore, only the CCM and dynamic behavior is considered here. Three operation states of the converter are:

- Supply the load using PV and FC while the battery is disconnected.

- Supply the load using PV, FC and battery, all together. (Battery is discharged)

- Supply the load using PV and FC, while the battery is charged.

These three operation states are analyzed and discussed below.
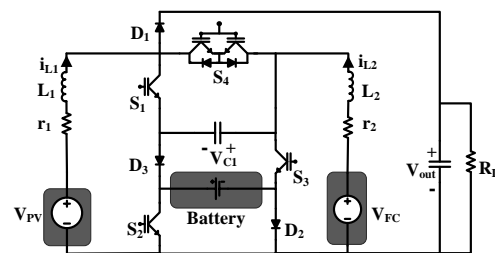
Fig. 2. The proposed multi-port DC/DC boost converter composed of PV/FC/Battery.

A. Operation state I: supply the load using PV and FC while the battery is disconnected.

Figure 3 (a)-(c) demonstrates three possible switching states along with paths of current flow. On the other hand, Fig. 3 (d) illustrates voltage waveform of inductors L_1 and L_2 as well as their current waveform while Ts is the sampling period and Dn (n=1, 2, 3) represents duty ratio of switching mode n.

First switching mode $(0<t<d_1Ts)$: In this

subinterval, S1 and S3 are ON while S2 is OFF. The inductors L1 and L2 charge with the positive voltage equal to $V_{PV}+V_{C1}$ and V_{FC} respectively. In addition, the output capacitor supplies the load [See Fig. 3 (a)].

Second switching mode ($d_1T_s <t< (d_1+d_2)T_s$): In this subinterval, as long as S3 is ON, S_1 and S_2 are OFF. The voltage across L_1 equals to $V_{PV}-V_{out}$, therefore L_1 is discharging while the inductor L_2 charges with the voltage of V_{FC}. In addition, the output capacitor is charged by the inductor current i_{L1} [See Fig. 3 (b)].

Third switching mode (($d_1+d_2)T_s <t<T_s$): In this subinterval, S_1 and S_3 are OFF and S_2 is ON. L_1 and L_2 are discharged until their voltage value equals to $V_{PV}-V_{out}$ and $V_{FC}-V_{C1}$, respectively. In addition, Fig. 3 (c) shows that the output capacitor is charged through inductor current i_{L1}.
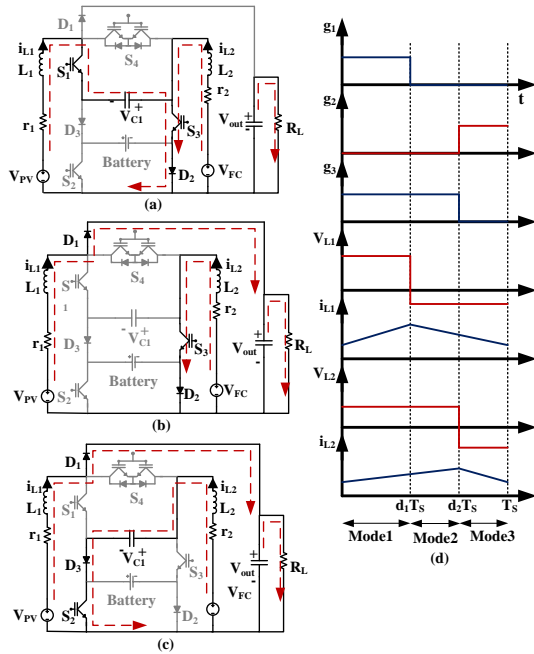
Fig. 3. Operation mode I: current path during a) first subinterval, b) second subinterval, c) third subinterval, d) switching commands and typical waveforms for inductors voltage and current.

Utilizing the balance principles of voltage-second and current-second to the proposed converter in this operation state, the following equations can be obtained:

Inductor L1:

$$d_1T_s(V_{PV} - r_1i_{L1} + V_{C1}) + (d_2 + d_3)T_s(V_{PV} - r_1i_{L1} - V_{out}) = 0 \quad (1)$$
$$V_{out} = \frac{V_{PV} - r_1i_{L1} + d_1V_{C1}}{d_2 + d_3}$$

Inductor L2:

$$(d_1 + d_2)T_s(V_{FC} - r_2i_{L2}) + d_3T_s(V_{FC} - r_2i_{L2} - V_{C1}) = 0$$
$$V_{C1} = \frac{V_{FC} - r_2i_{L2}}{d_3} \quad (2)$$

Battery:

$$i_{BATT} = 0 \rightarrow P_{BATT} = 0 \quad (3)$$

Capacitor C1:

$$d_1T_s(-i_{L1}) + d_3T_s(i_{L2}) = 0 \Rightarrow \frac{i_{L1}}{i_{L2}} = \frac{d_3}{d_1} \quad (4)$$

Capacitor CO:

$$d_1T_s(-I_O) + (d_2 + d_3)T_s(i_{L1} - I_O) = 0 \Rightarrow i_{L1} = \frac{1}{d_2 + d_3}I_O \quad (5)$$

Using (5) and (4), average value of L_2 is obtained as follows:

$$i_{L2} = \frac{d_1}{d_3(d_2 + d_3)}I_O \quad (6)$$

The voltage gain of the proposed converter in first operating mode is shown in Fig.4.
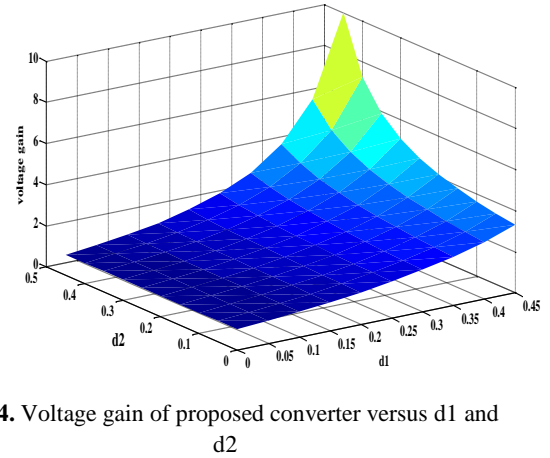
Fig. 4. Voltage gain of proposed converter versus d1 and d2

B. Operation state II: supply the load using power sources PV and FC and battery charging.
In this mode, PV and FC supplies the load as the generating sources. The battery is also charged by both power sources PV and FC. Four switching states are possible. The first, third, and fourth switching modes are the same as first, second, and third switching modes in the operation state I, respectively. The second switching state is discussed in the following. Fig. 5 (a)-(d) represents paths of current flow for these three switching modes. Furthermore, voltage and current waveforms of the aforementioned converter are illustrated in Fig. 5 (e).

Second Switching mode ($d_1T_s <t< (d_1+d_2)T_s$): In

this subinterval, S_1 is ON as long as S_2 and S_3 are off. According to Fig. 5 (b), the inductor L_1 charges with the V_{PV}-V_{BATT} and the inductor L_2 discharges with V_{FC}-V_{BATT}-V_{C1}. In addition, the output capacitor supplies the load.

Utilizing the balance principles of voltage-second and current-second to the converter, the following equations can be obtained:

Inductor L_1:

$$d_1 T_s (V_{PV} - r_1 i_{L1} + V_{C1}) + d_2 T_s (V_{PV} - r_1 i_{L1} - V_{BATT})$$
$$+ (d_3 + d_4) T_s (V_{PV} - r_1 i_{L1} - V_{out}) = 0$$
$$V_{out} = \frac{V_{PV} - r_1 i_{L1} + d_1 V_{C1} - d_2 V_{BATT}}{d_3 + d_4} \tag{7}$$

Inductor L_2:

$$(d_1 + d_3) T_s (V_{FC} - r_2 i_{L2}) + d_2 T_s (V_{FC} - r_2 i_{L2} - V_{C1} - V_{BATT})$$
$$+ d_4 T_s (V_{FC} - r_2 i_{L2} - V_{C1}) = 0$$
$$V_{C1} = \frac{V_{FC} - r_2 i_{L2} - d_2 V_{BATT}}{d_2 + d_4} \tag{7}$$

Battery:

$$i_{BATT} = d_2 (i_{L1} + i_{L2}) \rightarrow P_{BATT} = d_2 (i_{L1} + i_{L2}) V_{BATT} \tag{8}$$

Capacitor C1:

$$d_1 T_s (-i_{L1}) + (d_2 + d_4) T_s (i_{L2}) = 0$$
$$\frac{i_{L1}}{i_{L2}} = \frac{d_2 + d_4}{d_1} \tag{9}$$

C. Operation state III: Feeding the load with power sources PV, FC and battery.

Generated power of this state through PV and FC is not enough to supply the load. So, it is required to discharge battery to supply needed power. Four switching states are possible in this mode, while the first, third, and fourth switching states are similar to first, second, and third switching states in the operation mode I, and the second switching state is discussed here. The paths of current flow for these three switching modes are represented in Fig. 6 (a)-(d) while their proportional current and voltage waveforms are depicted in Fig. 6 (e).

Second switching state ($d_1 T_s < t < (d_1 + d_2) T_s$): In this subinterval, S_2, S_3 and S_4 are ON while S_1 is OFF. The inductors L_1 and L_2 charge with the voltage of $V_{PV} + V_{BATT}$ and $V_{FC} + V_{BATT}$ respectively. The output capacitor supplies the load [See Fig. 6 (b)]. Similar to other switching states, relations for capacitor voltages and inductor currents can be obtained.
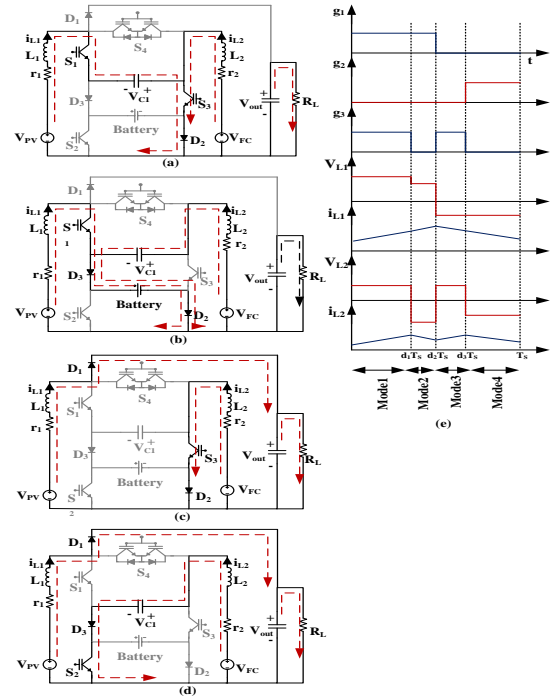
Fig. 5. Operation mode II: current path during a) first subinterval, b) second subinterval, c) third subinterval, d) forth subinterval, e) switching commands and typical waveforms for inductors voltage and current.

Inductor L_1:

$$d_1 T_s (V_{PV} - r_1 i_{L1} + V_{C1}) + d_2 T_s (V_{PV} - r_1 i_{L1} + V_{BATT})$$
$$+ (d_3 + d_4) T_s (V_{PV} - r_1 i_{L1} - V_{out}) = 0$$
$$V_{out} = \frac{V_{PV} - r_1 i_{L1} + d_1 V_{C1} + d_2 V_{BATT}}{d_3 + d_4} \tag{10}$$

Inductor L2:

$$(d_1 + d_3) T_s (V_{FC} - r_2 i_{L2}) + d_2 T_s (V_{FC} - r_2 i_{L2} + V_{BATT})$$
$$+ d_4 T_s (V_{FC} - r_2 i_{L2} - V_{C1}) = 0$$
$$V_{C1} = \frac{V_{FC} - r_2 i_{L_2} - d_2 V_{BATT}}{d_4} \tag{11}$$

Battery:

$$i_{BATT} = -d_2 (i_{L1} + i_{L2}) \rightarrow P_{BATT} = -d_2 (i_{L1} + i_{L2}) V_{BATT} \tag{12}$$

Capacitor C1:

$$d_1 T_s (-i_{L1}) + d_4 T_s (i_{L2}) = 0 \Rightarrow \frac{i_{L1}}{i_{L2}} = \frac{d_4}{d_1} \tag{13}$$

It should be noted that the proposed converter can also operate when there is only one input power source (only PV or only FC) which is easy to understand, and not discussed here for the sake of brevity.

3. SMALL SIGNAL MODEL AND CONTROL OF THE CONVERTER

It is necessary to study dynamic comportment of the converter to design its controller. To achieve this, small signal model of the understudying system is expressed bellow.
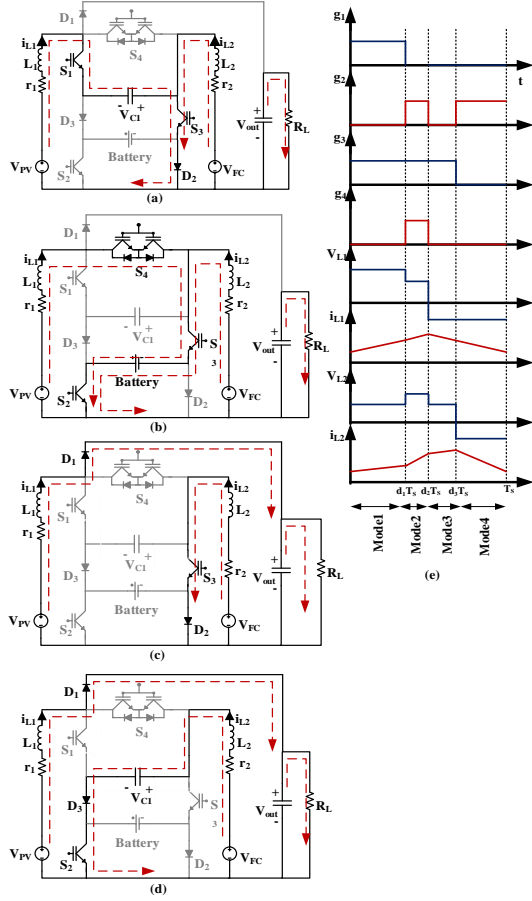
Fig. 6. Operation mode III: current path during a) first subinterval, b) second subinterval, c) third subinterval, d) forth subinterval, e) switching commands and typical waveforms for inductors voltage and current.

According to small signal technique [15], the state and control variables are composed of two parts: a DC value ($\bar{X}, \bar{D}$ Đ) and a perturbation ($\tilde{x}, \tilde{d}$ x̃đ) as below:

$$x = \bar{X} + \tilde{x}, d = \bar{D} + \tilde{d} \qquad (14)$$

$$\dot{\tilde{x}} = A\tilde{x} + B\tilde{u} \qquad (15)$$

$$\tilde{y} = C\tilde{x} + D\tilde{u}$$

Where $\tilde{x}, \tilde{d}$ and $\tilde{y}$ represents vector of state variable, control variables, and system output, respectively.

As described before, the presented converter is able to operate in three modes. It is necessary to set input generation sources and output voltage through various control variables in order to control the converter in each mode. This paper has introduced a

multi-input multi-output (MIMO) control system to be used in the converter. As a result of existing various interaction control loops in MIMO systems, it is hard to design closed-loop controllers for it. Although, decoupling network can be used in order to design apart closed-loop controllers for MIMO systems. As a result, small signal model of converter is required to design closed-loop controllers of the proposed MIC. This model is efficient in determining transient behavior, stability and appropriate design of controllers. iL1, iL2, VC1 and Vout are the state variables and the state space averaged model of the converter is as bellow.

A. Operation mode I
During this mode, two control variables d1 and d3, try to manage three state variables. So, the state-space averaged model is shown in:

$$L_1 \frac{di_{L1}}{dt} = V_{PV} - r_1 i_{L1} + d_1 V_{C1} - (1 - d_1)V_{out}$$

$$L_2 \frac{di_{L2}}{dt} = V_{FC} - r_2 i_{L2} - d_3 V_{C1}$$

$$C_1 \frac{dV_{C1}}{dt} = -d_1 i_{L1} + d_3 i_{L2} \qquad (16)$$

$$C_{out} \frac{dV_{Cout}}{dt} = \frac{-V_{out}}{R_L} + (1 - d_1)i_{L1}$$

B. Operation mode II
Here, d_1, d_2, and d_4 are controlled as control variables in order to set all of state variables. As a result, the state-space averaged model is given as:

$$L_1 \frac{di_{L1}}{dt} = V_{PV} - r_1 i_{L1} + d_1 V_{C1} - d_2 V_{BATT} - (1 - d_1 - d_2)V_{out}$$

$$L_2 \frac{di_{L2}}{dt} = V_{FC} - r_2 i_{L2} - (d_2 + d_4)V_{C1} - d_2 V_{BATT}$$

$$C_1 \frac{dV_{C1}}{dt} = -d_1 i_{L1} + (d_2 + d_4)i_{L2} \qquad (17)$$

$$C_{out} \frac{dV_{Cout}}{dt} = \frac{-V_{out}}{R_L} + (1 - d_1 - d_2)i_{L1}$$

C. Operation mode III
To manage all of state variables, the control variables d1, d2, and d3 are controlled. So, the state-space averaged model is given as:

$$L_1 \frac{di_{L1}}{dt} = V_{PV} - r_1 i_{L1} + d_1 V_{C1} + d_2 V_{BATT} - (1 - d_1 - d_2)V_{out}$$

$$L_2 \frac{di_{L2}}{dt} = V_{FC} - r_2 i_{L2} - d_4 V_{C1} + d_2 V_{BATT}$$

$$C_1 \frac{dV_{C1}}{dt} = -d_1 i_{L1} + d_4 i_{L2} \qquad (18)$$

$$C_{out} \frac{dV_{Cout}}{dt} = \frac{-V_{out}}{R_L} + (1 - d_1 - d_2)i_{L1}$$

According to equations (15) and (16), the matrix of

the small-signal models for three operating modes is obtained as:

Mode I:

$$A = \begin{bmatrix} -\dfrac{r_1}{L_1} & 0 & \dfrac{\bar{D}_1}{L_1} & \dfrac{\bar{D}_1-1}{L_1} \\[2mm] 0 & -\dfrac{r_2}{L_2} & \dfrac{-\bar{D}_3}{L_2} & 0 \\[2mm] \dfrac{\bar{D}_1}{C_1} & \dfrac{\bar{D}_3}{C_1} & 0 & 0 \\[2mm] \dfrac{1-\bar{D}_1}{C_{out}} & 0 & 0 & \dfrac{-1}{R_L C_{out}} \end{bmatrix} \quad B = \begin{bmatrix} \dfrac{\bar{V}_{C1}+\bar{V}_{out}}{L_1} & 0 \\[2mm] 0 & \dfrac{-\bar{V}_{C1}}{L_2} \\[2mm] \dfrac{-\bar{I}_{L_1}}{C_1} & \dfrac{\bar{I}_{L_2}}{C_1} \\[2mm] \dfrac{-\bar{I}_{L_1}}{C_{out}} & 0 \end{bmatrix}$$

$$\tilde{x} = \begin{bmatrix} \tilde{i}_{L_1} \\ \tilde{i}_{L_2} \\ \tilde{v}_{C1} \\ \tilde{v}_{out} \end{bmatrix} \quad \tilde{u} = \begin{bmatrix} \tilde{d}_1 \\ \tilde{d}_3 \end{bmatrix} \quad C = \begin{bmatrix} 1 & 0 & 0 & 0 \\ 0 & 0 & 0 & 0 \\ 0 & 0 & 0 & 0 \\ 0 & 0 & 0 & 1 \end{bmatrix} \quad D = 0 \tag{19}$$

According to the Eq. (20), G_{vd} relation is extracted. d_2 and d_3 values are considered constant. Equation (21) is ratio of the output voltage small perturbation to the d_1 small perturbation in operational point.

$$G_{Vd} = \frac{a_0 + a_1 S + a_2 S^2 + a_3 S^3}{b_0 + b_1 S + b_2 S^2 + b_3 S^3 + b_4 S^4}$$

$$a_0 = -R_L(V_{C1}+V_{out})(D_1-1)(D_1+D_2-1)^2$$

$$a_1 = -i_{L1}L_m R_L(D_1^2 + 2D_1 D_2 - D_1 + D_2^2 - 2D_2 + 1)$$

$$a_2 = -CL_m R_L(V_{C1}+V_{out})(D_1-1)$$

$$a_3 = -Ci_{L1}L_m^2 R_L$$

$$b_0 = R_L(D_1-1)^2(D_1+D_2-1)^2 \tag{20}$$

$$b_1 = L_m(2D_1^2 + 2D_1 D_2 - 2D_1 + D_2^2 - 2D_2 + 1)$$

$$b_2 = CL_m R_L(3D_1^2 + 2D_1 D_2 - 4D_1 + D_2^2 - 2D_2 + 2)$$

$$b_3 = CL_m^2$$

$$b_4 = C^2 L_m^2 R_L$$

Mode II:

$$A = \begin{bmatrix} -\dfrac{r_1}{L_1} & 0 & \dfrac{\bar{D}_1}{L_1} & \dfrac{\bar{D}_1+\bar{D}_2-1}{L_1} \\[2mm] 0 & -\dfrac{r_2}{L_2} & \dfrac{-(\bar{D}_2+\bar{D}_4)}{L_2} & 0 \\[2mm] -\dfrac{\bar{D}_1}{C_1} & \dfrac{\bar{D}_2+\bar{D}_4}{C_1} & 0 & 0 \\[2mm] \dfrac{1-\bar{D}_1-\bar{D}_2}{C_{out}} & 0 & 0 & \dfrac{-1}{R_L C_{out}} \end{bmatrix} \tag{21}$$

$$B = \begin{bmatrix} \dfrac{\bar{V}_{out}+\bar{V}_{C1}}{L_1} & \dfrac{\bar{V}_{out}-\bar{V}_{BATT}}{L_1} & 0 \\[2mm] 0 & \dfrac{-\bar{V}_{C1}-\bar{V}_{BATT}}{L_2} & \dfrac{-\bar{V}_{C1}}{L_2} \\[2mm] \dfrac{-\bar{I}_{L_1}}{C_1} & \dfrac{\bar{I}_{L_2}}{C_1} & \dfrac{\bar{I}_{L_2}}{C_1} \\[2mm] \dfrac{-\bar{I}_{L_1}}{C_{out}} & \dfrac{-\bar{I}_{L_1}}{C_{out}} & 0 \end{bmatrix} \quad C = \begin{bmatrix} 1 & 0 & 0 & 0 \\ 0 & 1 & 0 & 0 \\ 0 & 0 & 0 & 0 \\ 0 & 0 & 0 & 1 \end{bmatrix} \quad D = 0$$

$$\tilde{x} = \begin{bmatrix} \tilde{i}_{L_1} \\ \tilde{i}_{L_2} \\ \tilde{v}_{C1} \\ \tilde{v}_{out} \end{bmatrix} \quad \tilde{u} = \begin{bmatrix} \tilde{d}_1 \\ \tilde{d}_2 \\ \tilde{d}_4 \end{bmatrix}$$

According to the Eq. (22), G_{vd} relation is extracted. d_2, d_3 and d_4 values are considered constant. Equation (23) is ratio of the output voltage small perturbation to the d_1 small perturbation in operational point.

$$G_{Vd} = \frac{a_0 + a_1 S + a_2 S^2 + a_3 S^3}{b_0 + b_1 S + b_2 S^2 + b_3 S^3 + b_4 S^4}$$

$$a_0 = -R_L(D_2+D_4)^2(V_{C1}+V_{out})(D_1+D_2-1) \tag{22}$$

$$a_1 = -i_{L1}L_m R_L(D_2^2 + 2D_2 D_4 - D_1 D_2 + D_4^2 + D_1)$$

$$a_2 = -CL_m R_L(V_{C1}+V_{out})(D_1+D_2-1)$$

$$a_3 = -Ci_{L1}L_m^2 R_L$$

$$b_0 = R_L(D_2+D_4)^2(D_1+D_2-1)^2$$

$$b_1 = L_m(D_1^2 + D_2^2 + 2D_2 D_4 + D_4^2)$$

$$b_2 = CL_m R_L(2D_1^2 + 2D_1 D_2 - 2D_1 + 2D_2^2$$

$$+2D_2 D_4 - 2D_2 + D_4^2 + 1)$$

$$b_3 = CL_m^2$$

$$b_4 = C^2 L_m^2 R_L$$

Mode III:

$$A = \begin{bmatrix} -\dfrac{r_1}{L_1} & 0 & \dfrac{\bar{D}_1}{L_1} & \dfrac{\bar{D}_1+\bar{D}_2-1}{L_1} \\[2mm] 0 & -\dfrac{r_2}{L_2} & \dfrac{-\bar{D}_4}{L_2} & 0 \\[2mm] -\dfrac{\bar{D}_1}{C_1} & \dfrac{\bar{D}_4}{C_1} & 0 & 0 \\[2mm] \dfrac{1-\bar{D}_1-\bar{D}_2}{C_{out}} & 0 & 0 & \dfrac{-1}{R_L C_{out}} \end{bmatrix}$$

$$B = \begin{bmatrix} \dfrac{\bar{V}_{out}+\bar{V}_{C1}}{L_1} & \dfrac{\bar{V}_{out}-\bar{V}_{BATT}}{L_1} & 0 \\[2mm] 0 & \dfrac{\bar{V}_{BATT}}{L_2} & \dfrac{-\bar{V}_{C1}}{L_2} \\[2mm] \dfrac{-\bar{I}_{L_1}}{C_1} & 0 & \dfrac{\bar{I}_{L_2}}{C_1} \\[2mm] \dfrac{-\bar{I}_{L_1}}{C_{out}} & \dfrac{-\bar{I}_{L_1}}{C_{out}} & 0 \end{bmatrix} \quad C = \begin{bmatrix} 1 & 0 & 0 & 0 \\ 0 & 1 & 0 & 0 \\ 0 & 0 & 0 & 0 \\ 0 & 0 & 0 & 1 \end{bmatrix} \quad D = 0 \tag{23}$$

$$\tilde{x} = \begin{bmatrix} \tilde{i}_{L_1} \\ \tilde{i}_{L_2} \\ \tilde{v}_{C1} \\ \tilde{v}_{out} \end{bmatrix} \quad \tilde{u} = \begin{bmatrix} \tilde{d}_1 \\ \tilde{d}_2 \\ \tilde{d}_4 \end{bmatrix}$$

According to the Eq. (24), G_{vd} relation is extracted. d_2, d_3 and d_4 values are considered constant. Equation (25) is ratio of the output voltage small perturbation to the d_1 small perturbation in operational point.

$$G_{Vd} = \frac{a_0 + a_1 S + a_2 S^2 + a_3 S^3}{b_0 + b_1 S + b_2 S^2 + b_3 S^3 + b_4 S^4}$$

$$a_0 = -D_4^2 R_L(V_{C1}+V_{out})(D_1+D_2-1)$$

$$a_1 = -i_{L1}L_m R_L(D_4^2 + D_1 - D_1 D_2)$$

$$a_2 = -CL_m R_L(V_{C1}+V_{out})(D_1+D_2-1)$$

$$a_3 = -Ci_{L1}L_m^2 R_L$$

$$b_0 = D_4^2 R_L(D_1+D_2-1)^2$$

$$b_1 = L_m(D_1^2 + D_4^2)$$

$$b_2 = CL_m R_L(2D_1^2 + 2D_1 D_2 - 2D_1 + D_2^2$$

$$-2D_2 + D_4^2 + 1)$$

$$b_3 = CL_m^2 \tag{24}$$

$$b_4 = C^2 L_m^2 R_L$$

Utilizing the small signal model, the transfer function matrix proportional to the converter is as bellow:

$$G = C(SI - A)^{-1}B + D \qquad (25)$$

Converter stability can be verified using matrix Eigen values. The Eigen values of the matrix A equal to -0.3±1201.6j and -4.6±212.7j in a common operating point. As a result, aforementioned converter is stable in the referred operating point. The rank of the transfer function is determined based on the number of control variables. Since existence of two or three control variables, the transfer function of the multi-input multi-output (MIMO) is as bellow:

$$\begin{bmatrix} y_1 \\ y_2 \end{bmatrix} = \begin{bmatrix} g_{11} & g_{12} \\ g_{21} & g_{22} \end{bmatrix} \begin{bmatrix} u_1 \\ u_2 \end{bmatrix} \qquad (26)$$

$$\begin{bmatrix} y_1 \\ y_2 \\ y_3 \end{bmatrix} = \begin{bmatrix} g_{11} & g_{12} & g_{13} \\ g_{21} & g_{22} & g_{23} \\ g_{31} & g_{32} & g_{33} \end{bmatrix} \begin{bmatrix} u_1 \\ u_2 \\ u_3 \end{bmatrix} \qquad (27)$$

Figure 6 shows the transfer function (plant) of the system. From this figure, it can be seen that the control loops are coupled to each other, thus designing a close-loop compensator for each one is a difficult task. As a result, decoupling network can be utilized to design controller of each loop independently. So, a decoupling network is applied which is represented in Fig. 7. According to decoupling network derivation [33], the state vector x can be written as $x=Gu^*$ where u^* is the modified input vector made up of duty ratios. Therefore, $x=GG^*u$. Based on modern control theory, to permit one control input to determine on output, GG^* must be a diagonal matrix. Based on $G^*=G^{-1}xu^{-1}$, decoupling matrixes G^* can be written as:

$$G^* = \begin{bmatrix} 1 & \dfrac{-g_{12}}{g_{11}} \\ \dfrac{-g_{21}}{g_{22}} & 1 \end{bmatrix} \qquad (28)$$

$$G^*_{3\times3} =$$

$$\begin{bmatrix} 1 & \dfrac{g_{13} \cdot g_{12} - g_{12} \cdot g_{33}}{g_{11} \cdot g_{33} - g_{13} \cdot g_{31}} & \dfrac{g_{12} \cdot g_{23} - g_{13} \cdot g_{22}}{g_{11} \cdot g_{22} - g_{12} \cdot g_{21}} \\ \dfrac{g_{23} \cdot g_{31} - g_{21} \cdot g_{33}}{g_{22} \cdot g_{33} - g_{23} \cdot g_{32}} & 1 & \dfrac{g_{13} \cdot g_{21} - g_{11} \cdot g_{23}}{g_{11} \cdot g_{22} - g_{12} \cdot g_{21}} \\ \dfrac{g_{21} \cdot g_{32} - g_{22} \cdot g_{31}}{g_{22} \cdot g_{33} - g_{23} \cdot g_{32}} & \dfrac{g_{12} \cdot g_{31} - g_{11} \cdot g_{32}}{g_{11} \cdot g_{33} - g_{13} \cdot g_{31}} & 1 \end{bmatrix} \qquad (29)$$

Cross-coupled two-loop control system G can be separated into two independent single-loop control systems via decoupling network G* as follows:

$$\frac{y_1}{u_1} = g_{11} - g_{12}\frac{g_{21}}{g_{22}} \qquad (30)$$

$$\frac{y_2}{u_2} = -g_{12}\frac{g_{21}}{g_{11}} + g_{22} \qquad (31)$$

$$\frac{y_1}{u_1} = g_{11} + g_{12}\frac{g_{13} \cdot g_{32} - g_{12} \cdot g_{33}}{g_{11} \cdot g_{33} - g_{13} \cdot g_{31}} + g_{13}\frac{g_{12} \cdot g_{23} - g_{13} \cdot g_{22}}{g_{11} \cdot g_{22} - g_{12} \cdot g_{21}}$$

$$\frac{y_2}{u_2} = g_{21}\frac{g_{23} \cdot g_{31} - g_{21} \cdot g_{33}}{g_{22} \cdot g_{33} - g_{23} \cdot g_{32}} + g_{22} + g_{23}\frac{g_{13} \cdot g_{21} - g_{11} \cdot g_{23}}{g_{11} \cdot g_{22} - g_{12} \cdot g_{21}} \qquad (32)$$

$$\frac{y_3}{u_3} = g_{31}\frac{g_{21} \cdot g_{32} - g_{22} \cdot g_{31}}{g_{22} \cdot g_{33} - g_{23} \cdot g_{32}} + g_{13}\frac{g_{12} \cdot g_{31} - g_{11} \cdot g_{32}}{g_{11} \cdot g_{33} - g_{13} \cdot g_{31}} + g_{33}$$

Fig. 6 illustrates the thorough control strategy.

(a)

(b)

(c)
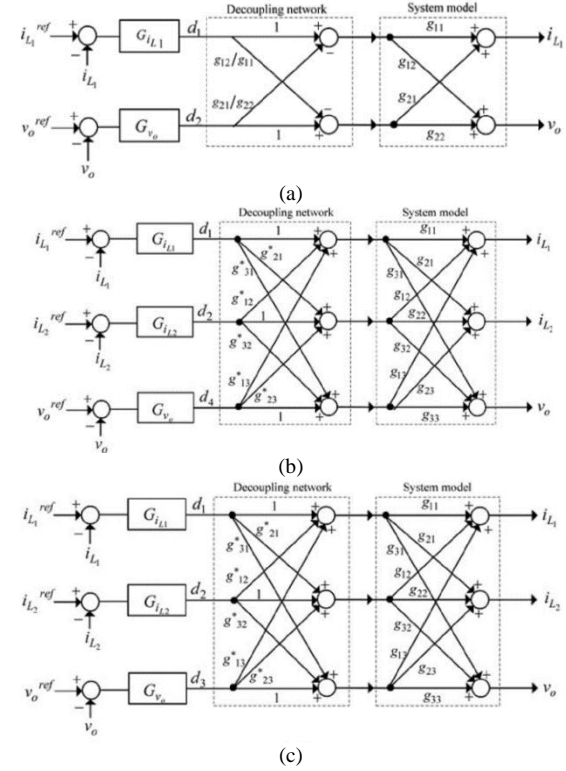
Fig. 7. Converter model along with decoupling network and closed-loop compensators in (a) mode I, (b) mode II, and (c) mode III

4. SIMULATION AND EXPERIMENTAL RESULTS

Several simulations are performed in MATLAB/Simulink software to evaluate the operation of the presented multi-input converter. Then, According to the Bode diagram, PI controller for all three operating mode is designed. In the following the P&O algorithm which is one of MPPT algorithms, is applied to the converter in operational mode I. An experimental prototype of the converter is provided while several tests have been performed. Simulation and experimental parameters are provided in Table 1. According to three operation modes of the presented converter, simulations are carried out in three steps. The operation mode of the presented converter is related to generated power of PV and FC. While the generated power is adequate to supply the load, operation of battery is not necessary. Otherwise, while the generated power of PV and FC are not

enough, it is essential to discharge the battery in order to supply the load. When battery requires to be charged, and the generated power of PV and FC is more than required power of the demanded load, the extra power will charge the battery. The switching frequency is fixed at 50 kHz.

Operation mode I: In this operation state, PV and FC are utilized to supply the load. Voltage of DC link is adjusted to be fixed at 450 V. The consumed power is 2 Kw .Fig. 8 and Fig. 9 represent the simulation results. The voltages across the capacitors are illustrated in Fig. 8 (a). According to this figure, voltage of output capacitor (DC-link voltage) is fixed at 450 Volt. Also, the voltage of the capacitor C_1 is about 250 V. The generated powers of different sources are shown in Fig. 8 (b). As it is shown, the sum of power supplies the output load. The currents flow from the sources are also shown in Fig. 8 (c). As it is shown, the battery does not operate in this operation state. The current flowing from the FC has a very low ripple which improves the efficiency of the FC. Power switches are selected according to voltage stress of main switches. The voltage stress waveform proportional to each switch is illustrated in Fig. 9. By assuming 450 V as the output voltage, these voltage stress values are reasonable and acceptable.

Operation mode II (PV, FC and Battery charging): Through this state, PV along with FC is employed to supply while the surplus generated power is utilized to charge the battery. Similar to mode I, according to Fig. 10 (a) the output DC link voltage equals to 450 V and demanded load power is still 2000 W. Fig. 10 (b) depicts the generation powers of the sources. As shown in this figure, battery power is not zero. The currents flowing from the sources are represented in Fig. 10 (c). According to this figure, battery current has fluctuations while Fig. 11 shows the voltage stresses on the switches.

Operation mode III (PV, FC and Battery discharging): In this operation mode, the load cannot be supplied only by the PV and FC. Therefore, the load is supplied by

Table 1. The experimental and simulation parameters.

Parameter	Value mode I	Value mode II	Value mode III
V_{PV}	50V	50V	50V
V_{FC}	80V	80V	80V
V_{BATT}	24V	24V	24V
D_1	0.57	0.575	0.51
D_2	0.115	0.05	0.05
D_3	0.315	0.05	0.16
D_4	None	0.325	0.28
C_1	10μF	10μF	10μF
C_{out}	1000μF	1000μF	1000μF
L_1	5mH	5mH	5mH
L_2	5mH	5mH	5mH
f	50kHz	50kHz	50kHz
R_L	100Ω	100Ω	100Ω
i_{L1}	5.2A	6A	5.2A
i_{L2}	9.4A	9.2A	9.3A
V_{C_1}	250V	210V	288V
V_{out}	450V	450V	450V
Proportional (P)	1.6653e-8	3.6273e-8	3.9183e-8
Integral (I)	0.0016653	0.0036273	0.0039183
Parameter	Experimental Value		
L_1	5mH		
L_2	5mH		
C_1	47μF		
C_{out}	220μF		
V_{PV}	50V		
V_{FC}	80V		
R_L	200Ω		
f	50kHz		
V_{out}	200V		

discharging the battery. Voltage of output DC link equals to 450 V and demanded load is 2000 W. The output powers of the sources are shown in Fig. 12 (b). As shown in this figure, the power of the battery is not zero and negative. Fig. 12 (c) shows the currents flowing from the sources. Fig. 12 (c) approves fluctuations of battery current. Again, the voltage stresses on the switches are depicted in Fig. 13. The results are shown below.

The simulation results of the presented converter indicate that the converter is able to operate in different conditions. The results are in consistent with the analysis done in the previous sections. Also, the presented control strategy can control and regulate voltage of DC-link.

(a)

(b)

(c)

Fig. 8. Simulation results for operation mode I, a) Voltage of C_1 and V_{out}, b) Output power of PV panel, FC stack and battery (battery is disconnected), c) injected currents by PV panels, FC stacks, and battery.

(a)

(b)

(c)
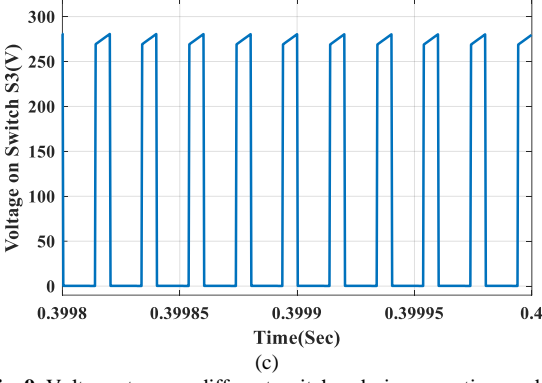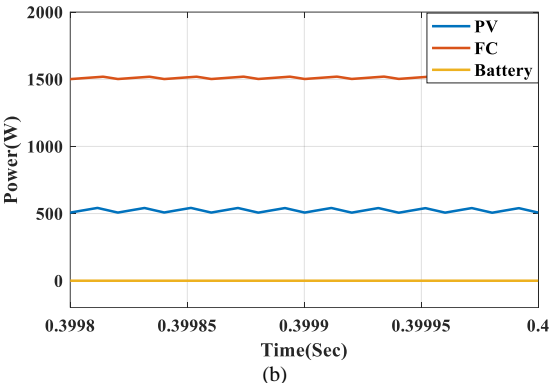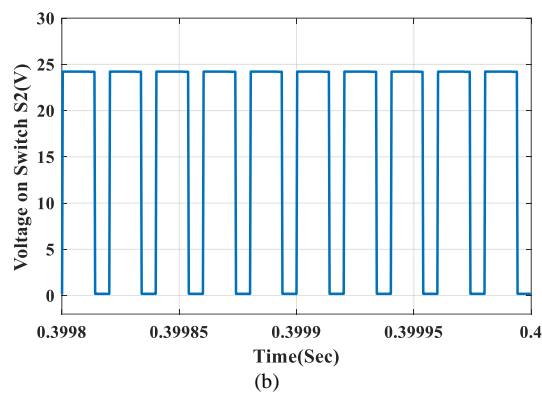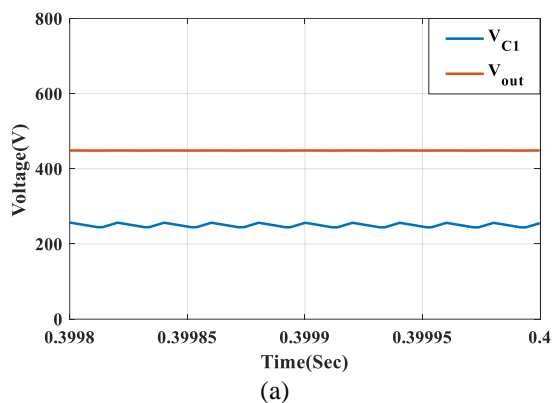
Fig. 9. Voltage stress on different switches during operation mode I, (a) Switch S_1, (b) Switch S_2, (c) Switch S_3.

(a)

(b)

(c)
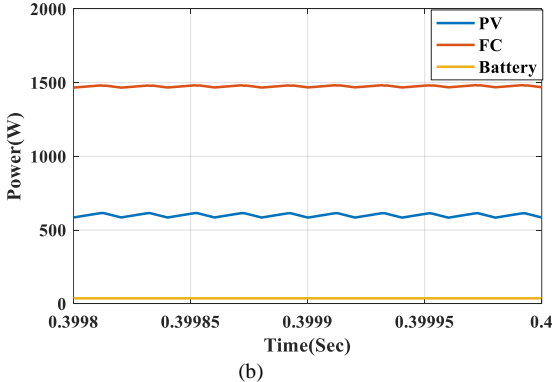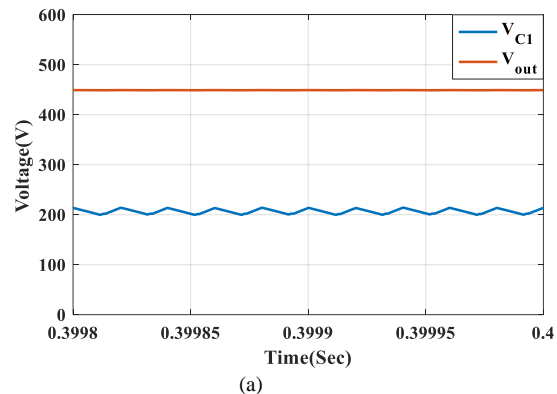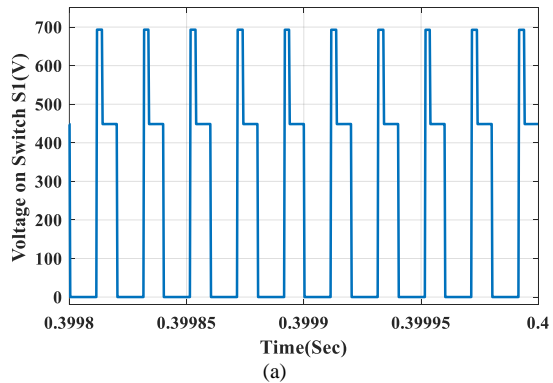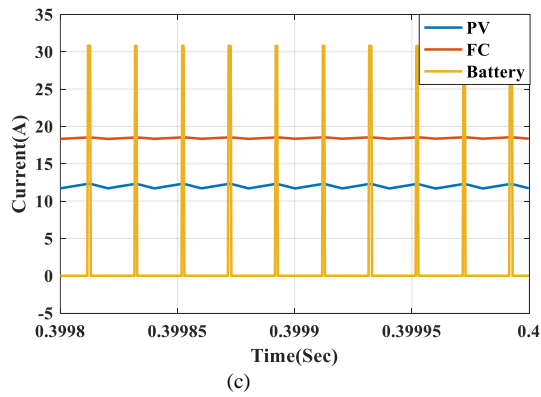
Fig. 10. Simulation results for operation mode II, a) Voltage of C_1 and V_{out}, b) Output power of PV panel, FC stack and battery, c) injected currents by PV panels, FC stacks, and battery.

(a)

(b)

(c)
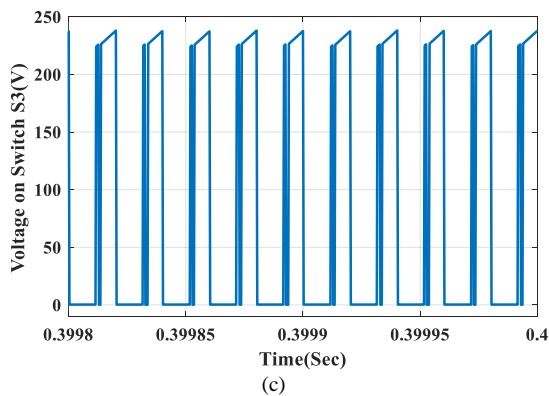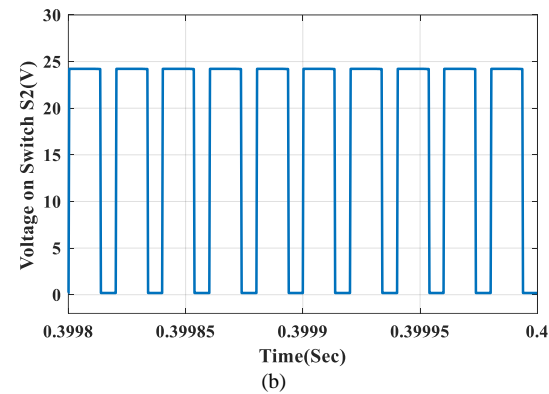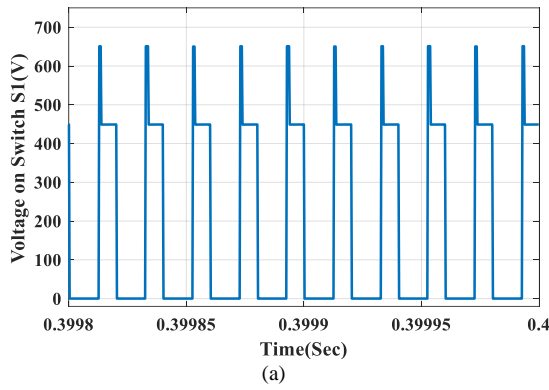
Fig. 11. Voltage stress on different switches during operation mode *II*, (a) Switch S_1, (b) Switch S_2, (c) Switch S_3.

(a)

(b)

(c)
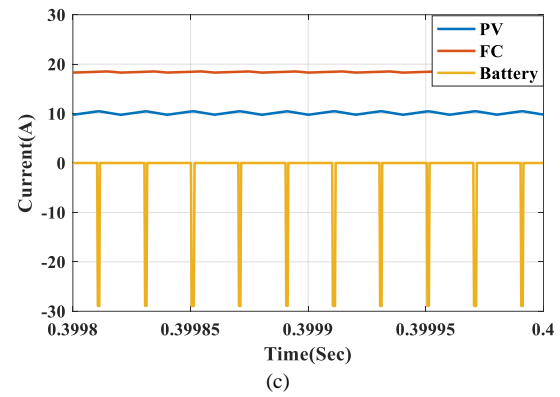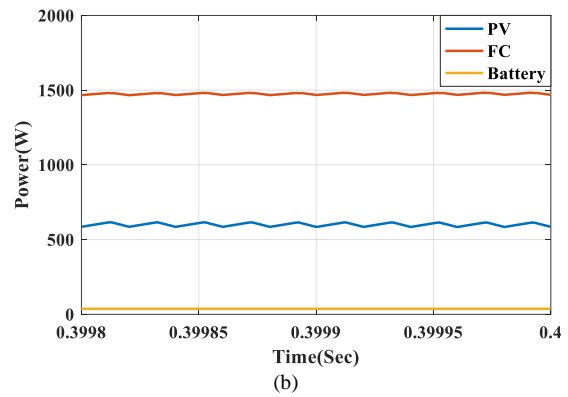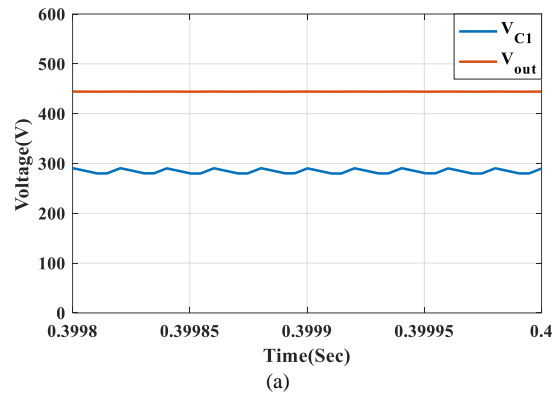
Fig. 12. Simulation results for operation mode III, a) Voltage of C_1 and V_{out}, b) Output power of PV panel, FC stack and battery, c) injected currents by PV panels, FC stacks, and battery.

(a)

(b)

(c)
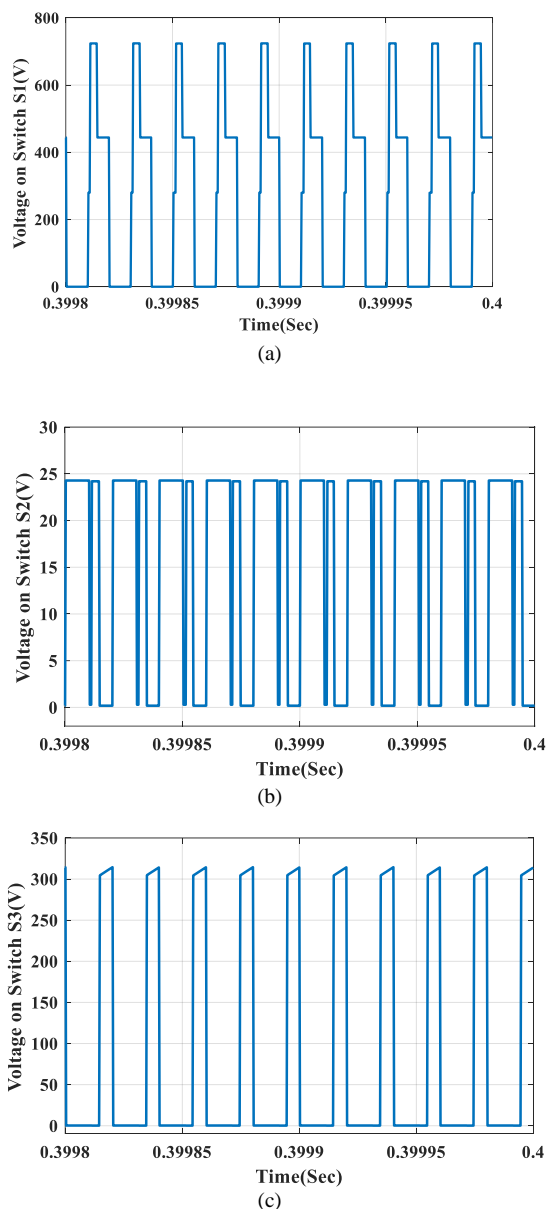
Fig. 13. Voltage stress on different switches during operation mode *III*, (a) Switch S_1, (b) Switch S_2, (c) Switch S_3.

In this section the PI controller is designed for all three operating modes.

According to Eq. (21) bode diagram for operational mode I is shown in Fig. 14. According to bode diagram, P and I coefficient for operating mode I are obtained and given in Table 1.The output of PI controller has d_1 value. d_2 and d_3 values are considered constant. The values of d_2 and d_3 are brought in Table 1. Simulation results for converter in operating mode I with PI controller are brought in Figs. 15 and 16.
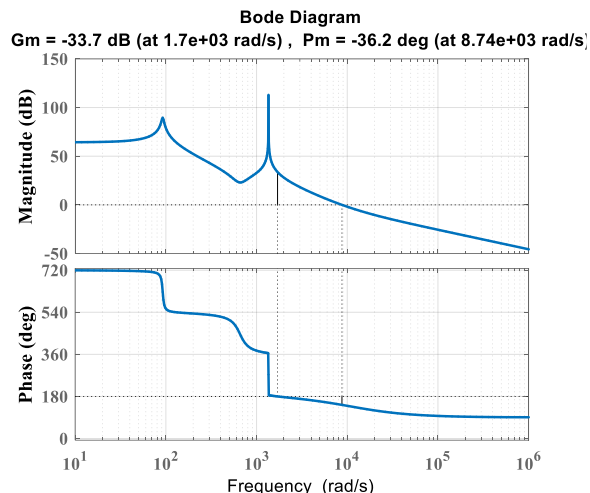
Fig. 14. G_{Vd} Bode diagram for operation mode I
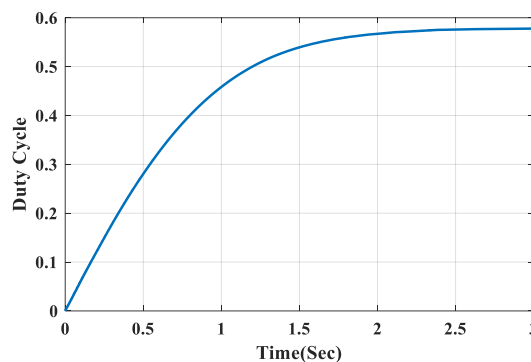
Fig. 15. Output of PI controller (D_1) for operation mode *I*
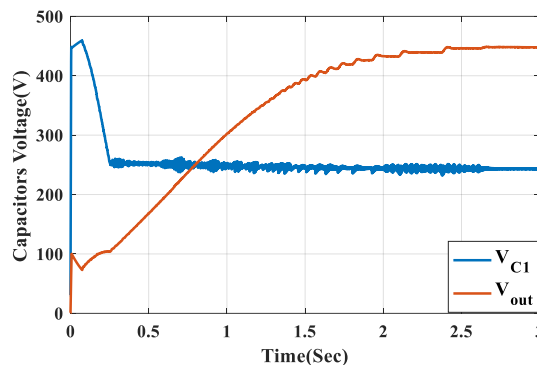
Fig. 16. Capacitors voltage for operation mode *I* with PI controller

According to Eq. (23) bode diagram for operational mode II is shown in Fig. 17. According to bode diagram, P and I coefficient for operating mode I are obtained and given in table (1) .The output of PI controller has d_1 value. d_2 , d_3 and d_4 values are considered constant. The values of d_2 , d_3 and d_4 are brought in Table 1. Simulation results for converter in operating mode II with PI controller are brought in Fig. 18 and Fig. 19.
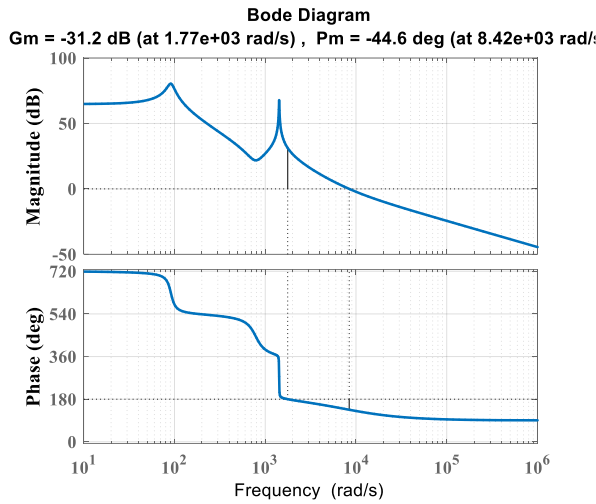
Fig. 17. G_{Vd} Bode diagram for operation mode II
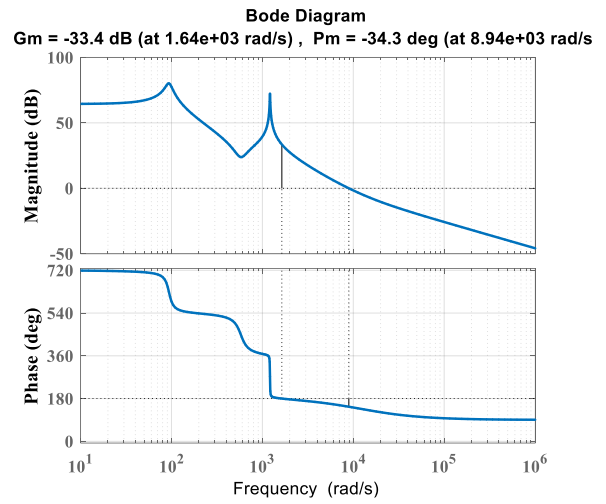
Fig. 20. G_{Vd} Bode diagram for operation mode III
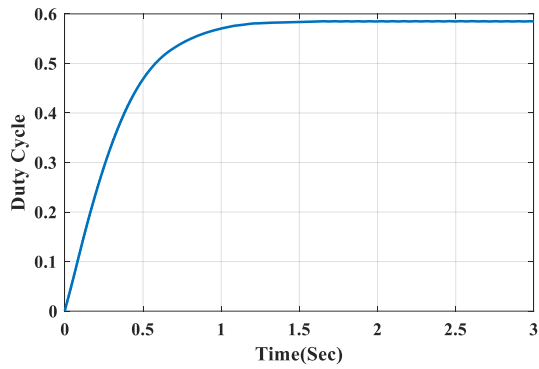
Fig. 18. Output of PI controller (D_1) for operation mode *II*
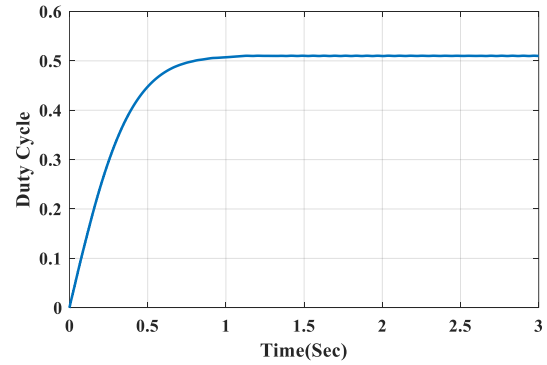
Fig. 21. Output of PI controller (D_1) for operation mode *III*
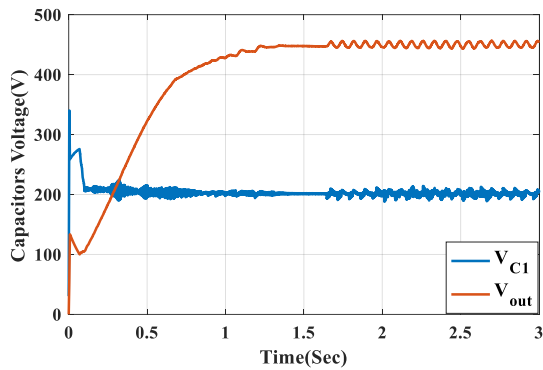
Fig. 19. Capacitors voltage for operation mode *II* with PI controller
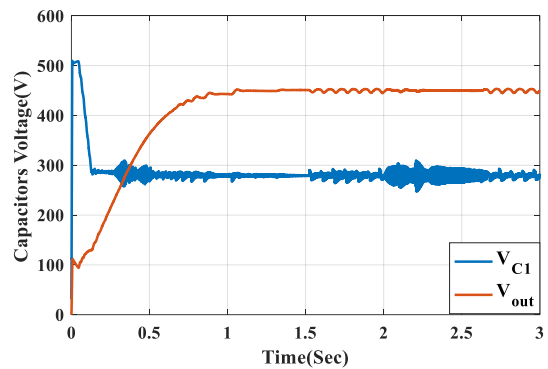
Fig. 22. Capacitors voltage for operation mode *III* with PI controller.

According to relation (25) Bode diagram for operational mode III is shown in Fig. 20. According to bode diagram ,P and I coefficient for operating mode I are obtained and given in Table 1.The output of pi controller has d_1 value. d_2 , d_3 and d_4 values are considered constant. The values of d_2 , d_3 and d_4 are brought in Table 1. Simulation results for converter in operating mode III with PI controller are brought in Figs. 21 and 22.

In this section P&O algorithm results are shown in operating mode I. Duty cycles of first and second switch are considered constant. The output of P&O algorithm has value of first switch duty cycle. Both of Power-current and power-time diagrams are brought in Figs. (23) and (24).
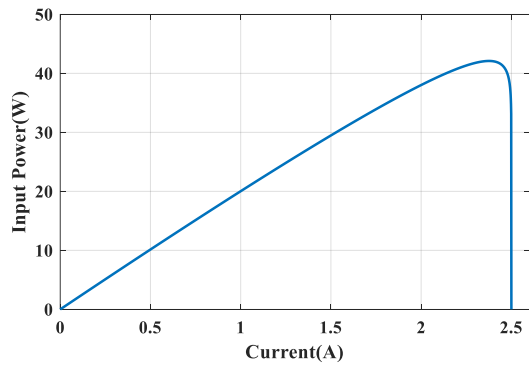
Fig. 23. Input power vs input current for PV panel.
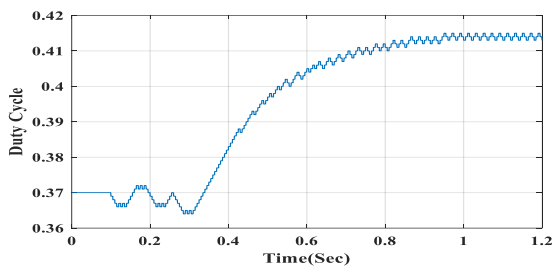
Fig. 24. Duty cycle of converter with MPPT algorithm
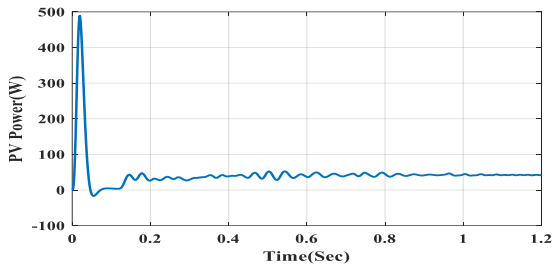
Fig. 25. PV Power with MPPT algorithm.

A laboratory prototype of system is implemented to show the practicability of proposed converter. The hardware implementation is shown in Fig.26.

Similar to simulations, the experimental results are obtained in different operation modes. All operation modes including:

1.   only PV and FC

2.   PV and FC with battery charging

3.   PV and FC with battery discharging

Results are provided in three cases as depicted in Fig. 27 and Fig. 28.

Fig. 26. Experimental prototype of the proposed converter.

(a)

(b)

(c)

(d)

(e)
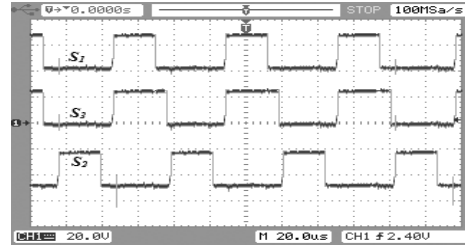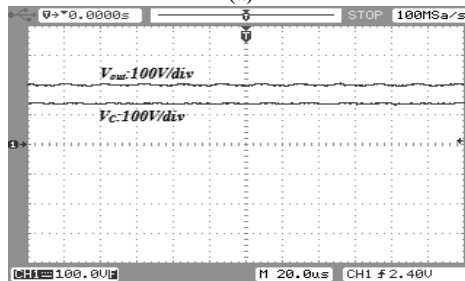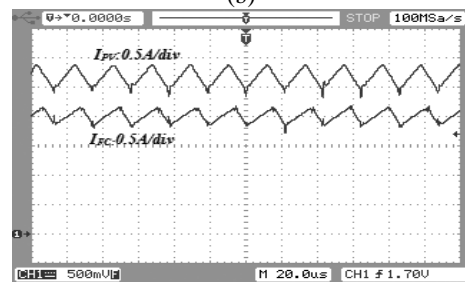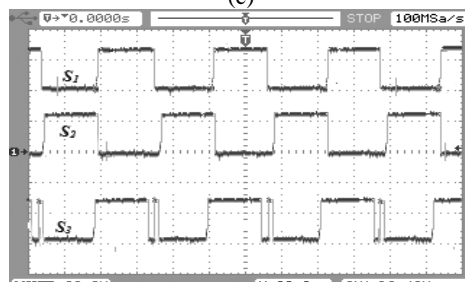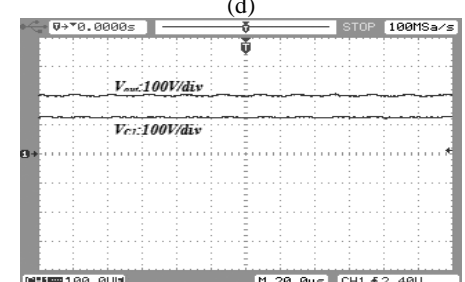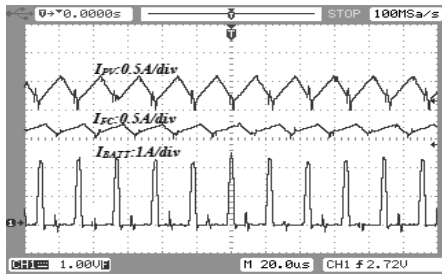
Fig. 27. Experimental results for operation modes *I* (a, b, and c) and *II* (d, e, and f), a)gate signals (10V/Div., 20 μsec/Div., b) output and C_1 voltages (50 V/Div.), c)inductor currents (0.5 A/Div.), d)gate signals (10V/Div., 20 μsec/Div., e) output and C_1 voltages (50 V/Div.), f)inductor currents (0.5 A/Div.).
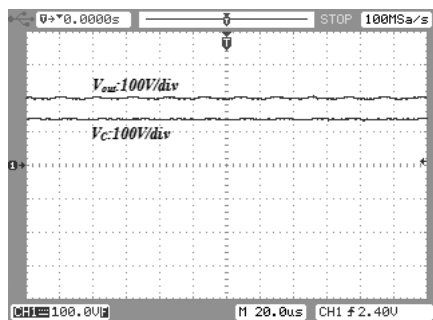
(a)
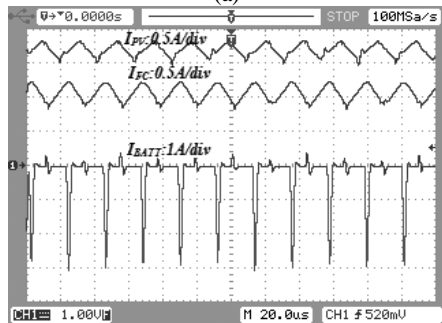
(b)

Fig. 28. Experimental result for operation mode *III*, a) output and C_1 voltages (50 V/Div.), b) inductor currents (0.5 A/Div.).

5. COMPARATIVE TUDY

A comparison study is done between proposed converter and converters in references [14- 17, 22, 23-25] and conventional boost converters in terms of number of inputs, number of inductors, number of power switches, number of diodes, number of capacitors and voltage gain. This study is given in Table 2. In this study it is assumed that the voltage of input power sources in multiport topologies are the same.

6. CONCLUSION

This paper has been devoted to propose a novel multi-port DC/DC boost converter. The proposed structure

is able to make various green energy sources able to supply a load. The presented converter has composed of two unidirectional power input ports as well as a bidirectional one. The converter has the capability of providing the demanded power by load in absence of one or two resources. The promising performance of the converter and employed control method offer a high reliability for utilizing the converter in industrial and domestic applications. Furthermore, steady state model of the converter and various operating modes have been discussed completely. In order to design an efficient controller, small signal model of the structure is extracted. Decoupling networks are used to design a more practical control strategy. Finally, simulation results have been presented to evaluate the accuracy confirm of the presented converter. Simulation results confirm the predominance of the proposed structure from view point of simplicity and efficient operation. The bode diagram has been plotted from the small signal model. Then the controller it was designed from the bode diagram. The results of simulation by the PI controller are presented. Also, the simulation results by P&O algorithm for the converter has been evaluated.

7. REFERENCES

[1]   W. D. Kellogg, M. H. Nehrir, G. Venkataramanan, and V. Gerez, "Generaton unit sizing and cost analysis for stand-alone wind, photovoltaic, and hybrid Wind/PV systems," *IEEE Trans. Energy Conv.*, vol. 13, no. 1, pp. 70-74, 1998.

[2]   S.H. Hosseini, A Farakhor, S. Khadem Haghighian, "Novel algorithm of MPPT for PV array based on variable step Newton-Raphson method through model predictive control," Proc. *13th Int. Conf. Control Autom. Syst.,* S. Korea, 2013, pp. 1577-1582.

[3]   F. Nakanishi, T. Ikegami, K. Ebihara, S. Kuriyama, and Y. Shiota, "Modeling and operation of a 10kW photovoltaic power generator using equivalent electric circuit method," Proc. *28th IEEE PV Syst. Conf.*, 2000, pp. 1703 -1706.

[4]   E. Babaei, and T. Ahmadzadeh. "A new structure of buck-boost z-source converter based on ZH converter." *J. Oper. Autom. Power Eng.*, vol. 4, no. 2, pp. 117-131, 2016.

[5]   I. Laird, H. Lovatt, N. Savvides, D. Lu, and V.G Agelidis, "Comparative study of maximum power point tracking algorithms for thermoelectric generators," Proc. *8th Australasian Uni. Power Eng. Conf.*, pp.1-6, 2008.

[6]   K. Jin, X. Ruan, M. Yang, and M. Xu, "A hybrid fuel cell power system," *IEEE Trans. Power Deliv.*, vol. 56, no. 4, pp. 1212-1222, Apr. 2009.

[7]   N. Kato, K. Kurozumi, N. Susuld, and S. Muroyama, "Hybrid power-supply system composed of photovoltaic and fuel-cell systems," Proc. *Int. Telecom. Energy Conf.*, 2001, pp. 631-635.

Table 2. Comparison study.

converter	proposed	boost	Diode assisted	[14]	[15]	[16]	[17]	[22]	[23]	[24]	[25]
Limitation of the number of inputs	3	1	1	3	3	2	-	-	-	2	2
Number of switches	4	1	1	4	4	4	3	2	2	4	3
Number of diodes	3	1	2	5	4	4	1	1	2	2	5
Number of capacitors	1	-	2	2	1	0	1	0	0	0	2
Number of inductors	2	1	2	2	2	2	2	1	2	2	2
Total device count	10	3	7	13	11	10	7	4	6	8	12
Voltage gain	$\dfrac{1-d_2}{(1-d_1)(1-d_1-d_2)}$	$\dfrac{1}{1-D}$	$\dfrac{1+D}{1-D}$	$\dfrac{1+d_2}{(1-d_2)(d_2-d_1)}$	$\dfrac{1-d_2+d_1d_2}{(1-d_1)(1-d_2)}$	$\dfrac{1}{1-D}$	$\dfrac{1}{1-D}$	$\dfrac{1}{1-D}$	$\dfrac{1}{1-D}$	$\dfrac{1}{1-D}$	$\dfrac{1+n}{1-D}$

[8] J.W. Jung, "Modeling and control of fuel cell based distributed generation systems" *PhD Thesis*, The Ohio State University, 2005.

[9] S. Jalilzadeh, A. Rohani, H. Kord, and M. Nemati, "Optimal design of a hybrid Photovoltaic/FC energy system for stand-alone application," Proc. IEEE , L'Aquila, Italy, 2009, pp. 1036–1041.

[10] E. Babaei, M. Baruji, H. Mashinchi Maheri, and A. Abbasnezhad, "A developed structure of step-up DC/DC converter by using coupled inductor and active clamped circuit." *J. Oper. Autom. Power Eng.,* vol. 5, no.1, pp. 31-42, 2017.

[11] C. Wang and M. H. Nehrir, "Power management of a stand-alone Wind/Photovoltaic/Fuel cell energy system," *IEEE Trans. Energy Conv.*, vol. 23, no. 3, pp. 957-967, Sept. 2008.

[12] O. C. Onara, M. Uzunoglu, and M. S. Alam, "Modeling, control and simulation of an autonomous wind turbine/photovoltaic/fuel cell/ultra capacitor hybrid power system," *J. Power Sour.*, vol. 185, no. 2, pp. 1273-1283, Apr. 2008.

[13] F. Z. Peng, H. Li, G. J. Su, and J. S. Lawler, "A new ZVS bidirectional dc-dc converter for fuel cell and battery application," *IEEE Trans. Power Electron.*, vol. 19, no. 1, pp. 54-65, Jan. 2004.

[14] R. R. Ahrabi, H. Ardi, M. Elmi and A. Ajami, "A novel step-up multiinput DC–DC converter for hybrid electric vehicles application," *IEEE Trans. Power Electron.*, vol. 32, no. 5, pp. 3549-3561, May 2017.

[15] F. Kardan, R. Alizadeh and M. R. Banaei, "A new three input DC/DC converter for hybrid PV/FC/Battery applications," *IEEE J. Emerging Sel. Top. Power Electron.*, vol. 5, no. 4, pp. 1771-1778, Dec. 2017.

[16] F. Nejabatkhah, S. Danyali, S.H. Hosseini, M. Sabahi, S.M. Niapour , "Modeling and control of a new three-input DC–DC boost converter for hybrid PV/FC/Battery power system," *IEEE Trans. Power Electron.*, vol. 27, no. 5, pp. 2309- 2324, 2012.

[17] S. Danyali, S.H. Hosseini, G.B. Gharehpetian, "New extendable single-stage multi-input DC–DC/AC boost converter," *IEEE Trans. Power Electron.*, vol. 29, no. 2, pp. 775-788, 2014.

[18] H. Krishnaswami and N. Mohan, "Three-port series-resonant DC-DC converter to interface renewable energy sources with bidirectional load and energy storage ports," *IEEE Trans. Power Electron.*, vol. 24, no. 10, pp. 2289-2297, 2010.

[19] K. Gummi, M. Ferdowsi, "Double-input DC–DC power electronic converters for electric-drive vehicles topology exploration and synthesis using a single-pole triple-throw switch," *IEEE Trans. Ind. Electron.*, vol. 57, no. 2, pp. 617-623, Feb. 2010.

[20] R.-J. Wai, S.-J. Jhung, J.-J. Liaw and Y.-R. Chang. "Intelligent optimal energy management system for hybrid power sources including fuel cell and battery," *IEEE Trans. Power Electron.*, vol. 28, no. 7, pp. 3231-3244, 2013.

[21] S. Kelouwani, N. Henao, K. Agbossou, Y. Dube, and L. Boulon. "Twolayer energy-management architecture for a fuel cell hev using road trip information," Vehicular Technology, *IEEE Trans.*, vol. 61, no. 9, pp. 3851-3864, Nov. 2012.

[22] R. J. Wai, C. Y. Lin, J. J. Liaw, Y. R. Chang, "Newly designed ZVS multi-input converter," *IEEE Trans. Ind. Electron.*, vol. 58, no. 2, pp. 555-566, Feb. 2011.

[23] R. J. Wai, B. H. Chen, "High-efficiency dual-input interleaved DC–DC converter for reversible power sources," *IEEE Trans. Power Electron.*, vol. 29, no. 6, pp. 2903-2921. Jun, 2014.

[24] S. H. Hosseini, S. Danyali, F. Nejabatkhah, "Multi-input DC boost converter for grid connected hybridPV/FC/Battery power system," Proc. *IEEE Elec. Ppwer Energy Conf.*, Canada, 2010, pp. 1-6.

[25] L. J. Chien, C. C. Chen, J. F. Chen, Y. P. Hsieh, "Novel three-port converter with high-voltage gain," *IEEE Trans. Power Electron.*, vol. 29, no. 9, pp. 4693-4703, Sep. 2014.